Low-cost fluoride adsorbents prepared from a renewable biowaste: Syntheses, Characterization and Modeling studies

S. Rajkumar, S. Murugesh, V. Sivasankar, A. Darchen, T. A. M. Msagati, T Chaabane

Arabian Journal of Chemistry (2019) 12, 3004–3017

King Saud University

Arabian Journal of Chemistry

www.ksu.edu.sa
www.sciencedirect.com

ORIGINAL ARTICLE

Low-cost fluoride adsorbents prepared from a renewable biowaste: Syntheses, characterization and modeling studies

S. Rajkumar [a], S. Murugesh [b], V. Sivasankar [c,*], A. Darchen [d], T.A.M. Msagati [e], T. Chaabane [f]

[a] *Department of Chemistry, Thiagarajar College of Engineering (Autonomous), Madurai 625 015, Tamil Nadu, India*
[b] *Department of Chemistry, Latha Mathavan Engineering College, Madurai 625 301, Tamil Nadu, India*
[c] *PG and Research Department of Chemistry, Pachaiyappa's College, Chennai 600 030, Tamil Nadu, India*
[d] *UMR CNRS n°6226 Institut des Sciences Chimiques de Rennes, ENSCR, 11 Allée de Beaulieu, CS 50837, 35708 Rennes Cedex 7, France*
[e] *University of South Africa, College of Science Engineering and Technology, UNISA Science Campus, 1709 Roodepoort, Johannesburg, South Africa*
[f] *University of Sciences and Technology Houari Boumediene, Faculty of Mechanical and Process Engineering/Environmental Department, BP 32 El-Alia 16111, Bab Ezzouar, Algiers, Algeria*

Received 18 March 2015; accepted 13 June 2015
Available online 4 July 2015

KEYWORDS

Cow dung carbon;
Defluoridation;
Fluoride removal;
Fluorophilic elements;
Adsorbent composite;
Adsorption

Abstract The preparation of composite adsorbents for fluoride anion was performed from natural cow dung and cow dung impregnated by a solution of calcium and iron salts. These starting materials were dried and carbonized at 300, 500 or 700 °C for 2 h leading to Cow Dung Carbon (CDC) or Ca–Fe Impregnated Cow Dung Carbon ICDC. All these carbons were used as adsorbent in fluoride removal studies. Batch mode experiments using CDC and ICDC were conducted in which the fluoride removal varied linearly as a function of contact time, pH, adsorbent dose, initial fluoride concentration, temperature and interfering anionic species. Both kinetic and isotherm based models were checked for the applicability of the present fluoride sorption system onto CDC and ICDC. For carbonization at 300 °C, the doping with Ca and Fe increased the defluoridation activity. The most efficient carbon was CDC which was prepared at 500 °C. It showed a defluoridation activity of 15 mg g^{-1}. This carbon was made from renewable cow dung without the need of a chemical activation. However, the recycling of F-loaded adsorbents may be carried out by washing in alkaline solution. CDC and ICDC were analyzed by scanning electron microscopy and X-ray diffraction in

* Corresponding author. Tel.: +91 4426412844; fax: +91 4426426900.
E-mail address: sivshri.20@gmail.com (V. Sivasankar).
Peer review under responsibility of King Saud University.

Production and hosting by Elsevier

http://dx.doi.org/10.1016/j.arabjc.2015.06.028

order to understand the reasons of their excellent defluoridation capacity. The growing of plants requires the consumption of essential inorganic nutrients such as Ca, Mg, and P which are known to be fluorophilic elements in fluoride adsorbents. After ingestion and digestion of plants by ruminants, some of these nutrients remained in cow dung and then in the corresponding carbonized materials where they acted as fluoride scavenger. This exceptional defluoridation capacity of CDC allows their use in rural countries.

1. Introduction

Occurrence of fluoride in groundwater has drawn worldwide attention due to its considerable impact on human physiology. The assimilation of fluoride into the human body from potable water at the level of 1.0 mg L^{-1} enhances bone development and prevents dental carriers. The maximum tolerance limit of fluoride in drinking water specified by the World Health Organisation (WHO, 2004) is 1.5 mg L^{-1}, but a lower concentration is recommended for children (Erdal and Buchanan, 2005). According to WHO estimate, excess fluoride concentration in groundwater (> 1.5 mg/L) is affecting more than 260 million people around the world (Amini et al., 2008). Even though the upper limit of fluoride concentration in drinking water is 1.5 mg L^{-1}, in many tropical countries, where there is a high sweat loss and a high intake of water due to the hot weather, such an upper limit may be unsuitable (Brouwer et al., 1988). The Bureau of India Standards (BIS) prescribes a limit between 1.0 and 1.5 mg L^{-1}. In India, about 62 million people are at risk of developing fluorosis from drinking fluoride contaminated water (Andezhath and Ghosh, 2000). Fluoride in human body mainly affects solid tissues depending on its exposure time and leads to dental fluorosis and skeletal fluorosis. Dental fluorosis is of particular concern during childhood when teeth are actively formed which leads to an increase in the porosity of enamel and decreases in mineral content. Excessive intake of fluoride damages enamel and leads to abnormal development of teeth (Hussain et al., 2004). Besides this cosmetic consequence of fluoride excess, the neurotoxicity of fluoride has been recently emphasized because it is more susceptible to injury developing human brains than the brain of an adult (Grandjean and Landrigan, 2006; Tang et al., 2008). Children who live in a fluorosis area have five times higher odds of developing low IQ than those who live in a slight fluorosis area. Owing to the toxicity of fluoride for children it is important to develop efficient and cheap defluoridation treatment of the water of fluorosis areas.

Fluoride removal methods can be divided into membrane and adsorption techniques. Membrane techniques include reverse osmosis (Meenakshi and Maheswari, 2006), nano-filtration (Tahaikt et al., 2007) and electrodialysis (Kabay et al., 2008). Adsorption techniques are easy to use and a lot of adsorbents have been investigated. They include low-cost compounds and more sophisticated ones: aluminum based materials (Tripathy et al., 2006) clays and soils (Chidambaram et al., 2013), calcium based minerals (Sasaki et al., 2013), synthetic compounds (Yu et al., 2013), seaweed species (Paudyal et al., 2013) and carbon based materials (Sivasankar et al., 2012a,b). Researchers have also worked on defluoridation using wastes of industrial and biotic origins. The fluoride sorption tendency of activated carbon from agricultural waste was attempted by Sivabalan et al. (2002) by batch and column mode experiments.

Preparations of carbonaceous adsorbents from various waste materials have been reviewed but their applications to fluoride removal are scarce (Bhatnagar and Sillanpää, 2010; Dias et al., 2007; Ioannidou and Zabaniotou, 2007). The preparation of carbon materials from natural sources and their fluoride removal capacity have been recently reviewed in an original paper (Mohan et al., 2012). The use of fluoride adsorbent carbons arising from carbonization of cow dung or cattle dung has not been reported yet. The utilization of cow dung in many forms is well known. In many parts of the world, the caked and dried cow dung for fuel application is well known (Aggarwal and Singh, 1984). Production of biogas and the generation of heat and electricity have drawn significant attention across the world using cow dung. Carbonization of cow or cattle dung is scarce (Demiral and Demiral, 2008; Das et al., 2000; Elaigwu et al., 2009; Bhattacharya and Yu, 2014) and the corresponding carbon materials have never been used in defluoridation. Adsorption activity of cow dung carbon has been investigated against Cr(VI) (Das et al., 2000) and Pb(II) (Elaigwu et al., 2009). A more recent application has been reported in the preparation of electrode materials (Bhattacharya and Yu, 2014).

In the present work, the application of cow dung carbon is extended as an adsorbent in the removal of fluoride from drinking water. The growing of plants requires the assimilation of essential inorganic nutrients that contain Ca, Mg and P. These elements are essential for herbivorous animals in the constitution of solid parts of their body such as bones and teeth. These elements are also known as fluorophilic elements in fluoride adsorbents. After ingestion and digestion of plants these elements are found in dung (Winterhalder et al., 1974) and then in the carbonized materials where they acted as fluoride scavenger. Since cow or cattle are widely present in rural countries cow or cattle dung carbons can be easily prepared without the use of chemicals and so it allows the access to quality water for poor people. The objective on fluoride removal was envisaged based on the carbon and calcium contents present in the cow dung.

2. Materials and methods

2.1. Chemicals and materials

All the chemicals used in the present study were of analar grade. Solutions were made with distilled water. Fresh cattle dung was collected from the study area called U. Vadipatty

village, Uthappanaikanur Firka in Usilampatty Taluk of Madurai District. It was air-dried for about 15 days under sunlight. The wet dung material was monitored and frequently stirred to facilitate the drying process and to avoid the growth of fungal attack as well.

2.2. Syntheses of sorbent carbons

The sun-dried cattle dung was sieved for the particle size of < 600 μm. Then 25 g of dried cattle dung was stirred with 0.2 L of a solution of 0.05 M $CaCl_2$ and 0.05 M $FeCl_3$ for 2 h. After stirring, the whole content was left undisturbed for 24 h for aging. After filtration, the impregnated wet mass was dried in hot air-oven maintained at 100 ± 5 °C for 3 h. The impregnated and dried material was carbonized by keeping in the muffle furnace at 300 °C, 500 °C or 700 °C for 2 h leading to Impregnated Cow Dung Carbon (ICDC). Simultaneously, the non-modified carbons such as CDC were prepared by stirring 25 g of sun-dried cattle dung in 0.2 L of distilled water, followed by the drying and carbonization processes. The virgin and modified carbons are abbreviated with reference to the mention of impregnation and carbonization temperature as follows: Cow Dung Carbonized at 300 °C, 500 °C or 700 °C is noted CDC@300 °C, CDC@500 °C or CDC@700 °C, respectively. Impregnated Cow Dung Carbonized at 300 °C, 500 °C or 700 °C is noted CDC_{CaFe}@300 °C, CDC_{CaFe}@500 °C or CDC_{CaFe}@700 °C, respectively.

2.3. Characterization of sorbent carbons

CDC and ICDC were observed and analyzed by Scanning Electron Microscope (SEM) and Energy Dispersive Spectroscopy (EDS) with a JEOL JSM model 5610 microscope to study its surface morphology. Powder X-ray diffraction (XRD) patterns were collected with a INEL XRG 3500 diffractometer using Cu Kα (λ = 1.540560 Å) at 30 kV and 30 mA with an angle range 2θ between 5° and 120° and step length of 0.02°(2θ). The specific surface of carbons was determined by nitrogen adsorption/desorption at 77.5 K on a Micromeritics ASAP 2020, V3.00H instrument. Elemental analysis was done by Micro-analyzer flash EA1112 CHNS/O from Thermo Electron. FTIR spectra were recorded with a Shimadzu IR – Prestige-21 instrument.

The iodine number of carbons was determined using the standard volumetric method carried out by iodometry. The pH of the point of zero charge pH_{PZC}, i.e. the pH above which the total surface of the carbon particles is negatively charged was measured by the so-called "pH drift method" (Newcombe et al., 1993). For this purpose, 0.05 L of a 0.01 M NaCl solution was placed in a jacketed titration vessel, thermostated at 298 K, and N_2 was bubbled through the solution to stabilize the pH by preventing the dissolution of CO_2. The pH was then adjusted to successive initial values between 2 and 12, by adding either HCl or NaOH and the carbon (0.1 g) was added to the solution. The final pH, reached after 48 h, was measured and plotted against the initial pH. The pH at which the final pH crosses the line $pH_{final} = pH_{initial}$ is taken as the pH_{PZC} of the given carbon.

The acidic and basic surface contents of carbons were determined using the Boehm's titration method (Boehm, 1994). A dried carbon sample (0.1 g) was mixed with 50 mL of 0.025 M NaOH or 0.020 M HCl under N_2 atmosphere. After 1 h of stirring and filtration, the excess of base and acid was titrated with 0.020 M HCl and 0.025 M NaOH, respectively. Surface acidity and basicity were calculated with the assumption that HCl and NaOH neutralize all basic groups and acidic groups, respectively.

2.4. Fluoride adsorption studies

Fluoride solutions were prepared by diluting a homemade stock NaF solution (100 mg of F^- L^{-1}). The defluoridation experiments were carried out by batch method at various temperatures 298 K, 308 K and 318 K. A defined quantity of 0.05 g of dry carbon was added into 0.05 L of a fluoride solution with a desired pH value. The pH of the medium was adjusted using either HCl or NaOH. An equilibrium time of 30 min was optimized for shaking and the residual fluoride concentration was determined thanks to a fluoride ion selective electrode (Orion, number BN 9609, USA) connected to an ion meter (Orion, model 290A, USA). The kinetic study was carried out at pH 7.50 ± 0.05 with different initial fluoride concentrations (2–8 mg L^{-1}) and temperatures (298 K, 308 K and 318 K). The effect of CDC@500 °C dose for fluoride uptake capacity was studied in the concentration range of 1.0–6.0 g L^{-1} with an initial fluoride concentration of 2 mg L^{-1}. The interference of various ions *viz*., Cl^-, HCO_3^-, NO_2^-, NO_3^- and SO_4^{2-} on fluoride sorption was also studied under the optimized conditions. Desorption study was attempted using the regenerating solutions of 0.05 M, 0.1 M and 0.2 M NaOH for the fluoride concentrations of 2–8 mg L^{-1}. Thermodynamic parameters of adsorption *viz*., free energy change (ΔG), enthalpy change (ΔH), entropy change (ΔS), sorption energy (E) and activation energy (E_a) were calculated. Eqs. (1)–(12) based on kinetics, isotherm and thermodynamics of sorption are given in Table 1.

3. Results and discussion

3.1. Characterizations of carbon materials

The non-modified carbon CDC@500 °C is a typical and the best material in this study, and for this reason the paper focuses on its characterizations and on the main effects of the Ca and Fe impregnation. Some results are shown in Table 2.

3.1.1. Chemical composition

Elemental analyses of CDC@500 °C (Table 2) revealed the presence of 31.21% of carbon which is closer to the study conducted by Prasad who reported the percentage of C, H and N in cattle dung (Prasad, 1993). But the decrease in the percentage of hydrogen and nitrogen in CDC@500 °C as compared to dried cattle dung may be associated with the release of water vapor and ammonia or nitrogen oxides during the carbonization process. The amount of substantial hydrogen and the amount of nitrogen were about 1.61% and 1.33% respectively with very small amounts of sulfur of 0.21%. The presence of oxygen and inorganic oxides in CDC@500 °C was about 65.64%. The substantial oxygen and inorganic residues of

Table 1 Kinetic, isotherm model equations and associated parameters.

Model	Equation	Plotting parameters as		Description and units	Ref.	Equation number
		X	*Y*			
Kinetic type						
1. Pseudo-first-order	$\ln(q_e - q) = \ln q_e - k_1(t)$	Time (t)	ln ($q_e - q$)	$k_1 \rightarrow$ Pseudo-first-order rate constant in min^{-1}	Lagergren (1898)	(1)
2. Pseudo-second-order	$dq/dt = k_2(q_e - q)^2$ $t/q_t = 1/k_2 q_e^2 + (1/q_e)t$	Time (t)	t/q_t	$k_2 \rightarrow$ Pseudo-second-order rate constant in g mg^{-1} min^{-1}; h ($=kq_e^2$) $\rightarrow$ initial sorption rate in mg g^{-1} min^{-1}	Ho et al. (1996)	(2) (3)
3. Intra-particle diffusion	$q_t = k_i t^{1/2} + C$	Time$^{1/2}$ $(t)^{1/2}$	q_t	$k_i \rightarrow$ intraparticle rate constant in mg g^{-1} $min^{-0.5}$; $C \rightarrow$ thickness of the boundary layer in mg g^{-1}	Weber and Morris (1964)	(4)
4. Elovich	$q_t = (1/B)\ln AB + (1/B)\ln t$	Time (t)	ln(t)	$A \rightarrow$ initial adsorption rate in mg $g^{-1}min^{-1}$; $B \rightarrow$ constant of desorption in g mg^{-1}	Aharoni and Tompkins (1970)	(5)
In the above kinetic models, q_t and q_e are the amount of fluoride adsorbed at time, t and equilibrium respectively in mg g^{-1}						
Isotherm type						
1. Langmuir	$q_e = Q^o bC_e/1 + bC_e$	C_e	q_e	$Q^o \rightarrow$ Sorption capacity in mg g^{-1}; $L \rightarrow$ Langmuir isotherm constant in L mg^{-1}	Langmuir (1916)	(6)
2. Freundlich	$q_e = K_F C_e^{1/n}$	$\log C_e$	$\log q_e$	$C_e \rightarrow$ equilibrium concentration of fluoride in solution in mg L^{-1}; $K_F \rightarrow$ adsorption capacity in mg g^{-1}; $1/n \rightarrow$ adsorption intensity or surface heterogeneity ($0.1 \leqslant 1/n \geqslant 1.0$ and $1 \leqslant n \geqslant 10 \rightarrow$ favorable for sorption	Freundlich (1906)	(7)
3. DKR	$Ln\, q_{ed} = \ln q_{md} - k\varepsilon^2$ $E = -1/\sqrt{-2\beta}$ $\varepsilon = RT\ln(1/C_e)$	ε^2	$\ln q_e$	q_{ed}-amount of fluoride adsorbed per unit weight of adsorbent (mmol g^{-1}) q_{md}-monolayer adsorption capacity (mmol g^{-1}) β-constant related to adsorption energy (mol^2 $(kJ)^{-1}$)	Dubinin and Radushkevich (1947)	(8) (9) (10)
Thermodynamic parameters						
1. Free energy of sorption	$\Delta G = -RT\ln K$ $\ln K = -\Delta H/RT + \Delta S/R$	$\ln q_e$	C_e	$\Delta G \rightarrow$ Free energy change in kJ mol^{-1}; $\Delta H \rightarrow$ Enthalpy change in kJ mol^{-1}; $\Delta S \rightarrow$ Entropy change in kJ mol^{-1} K^{-1}; $K \rightarrow$ Sorption equilibrium constant	Sepehr et al. (2013)	(11) (12)

Table 2 Properties of CDC@500 °C.

Elemental analysis in %	
Carbon	31.21
Hydrogen	1.61
Nitrogen	1.33
Sulfur	0.21
Oxygen + inorganic residues	65.64
Textural data	
Single point surface area ($m^2\ g^{-1}$)	18.3
BET surface area ($m^2\ g^{-1}$)	19.2
Total pore volume ($cm^3\ g^{-1}$)	0.092
Average pore width (nm)	19.2
Average pore diameter (nm) during	
BJH adsorption	18.3
BJH desorption	15.4
Iodine number (mg g^{-1})	912
pH_{zpc}	9.09

8–11% (by weight) in the carbonized material enhance the nature of hydrophilicity. The degree of carbonization may be described by the molar ratio of H/C because H is primarily associated with the organic matter (Kolodynska et al., 2012). The H/C and O/C molar ratios of CDC@500 °C were 0.62 and 1.58 respectively. The H/C ratio suggests that the cattle dung is weakly carbonized but, based on the O/C ratio it is found to contain high polar group contents which could facilitate the formation of water clusters on carbon surface (Lesmana et al., 2009).

The inorganic oxides formed due to calcium, magnesium, iron and silicon get hydroxylated and develop a surface charge in aqueous medium. From EDS results, it was observed that carbons undergo changes in their elemental compositions between the carbonization temperatures 300 °C and 500 °C. The increase in carbonization temperature increased the loss of carbon and led the carbon content reduction from 59% to 25% at 700 °C. Conversely, the percentage of oxygen and other inorganic oxides was appreciably increased from 30% to 51%. Oh et al. (2012) inferred the loss of oxygen and hydrogen due to dehydration (as surface functional – OH groups) and structural rupture of C—O and O—H groups at 700 °C under oxygen limited conditions. But in the present study, under excess supply of oxygen, the presence of undigested cellulose, hemi-cellulose, lignin and other nitrogenous compounds in metabolic excretions gets converted into the carbonized form along with other inorganic oxides. The decrease in the carbon content was facilitated under roasting against its increase under carbonization (Shen et al., 2011). Similar result on the preparation of activated carbon with decreasing carbon content was reported during carbonization in nitrogen atmosphere (Demiral et al., 2011). In support of our results, the carbon content decrease was observed for synthesized charcoals during the increase of the carbonization temperature from 500 °C to 900 °C (Tchomgui-Kamga et al., 2010a,b).

3.1.2. Porous structure

Nitrogen isotherms were carried out to evaluate the specific surface area and pore size distribution of CDC@500 °C. The general shape of the nitrogen sorption isotherm indicated the size of different pore sizes which varied between micropores and mesopores. At low relative pressure area ($P/P_o < 1$) the graph (Fig. 1A) showing hysteresis represents a drastic uptake which reveals the presence of micropores. Meanwhile, slight uptake at higher relative pressures nearby 1 corroborated the existence of macropores which is likely between particles. The graph resembles the type II and type III isotherms which evidence the existence of particles with micro- and mesoporous nature wherein the amount of adsorption increases without limit and its natural adsorption approaches unity.

Pores include primary (< 8 Å) and secondary micropores (8–20 Å width), mesopores (20–500 Å width) and macropores (> 500 Å width). Macropores represent the entrance to the internal adsorbent pore structure, and mesopores facilitate diffusive transport to adsorption sites. The micropores are hosts for most pollutants. Activated carbon contains macropores close to the surface that branch into mesopores and finally micropores. In the graph, it is very clear that the curve which ascends up to 0.1 is followed by a plateau up to 0.7–0.8. This positive plateau falls between the relative pressures 0.1 and 0.8 indicates the development of mesopores. The curve of relative pressure finally ends with an upward sweep occurring near the saturation pressure ($P/P_o = 1$).

CDC@500 °C exhibited a pore size distribution depicted (Fig. 1B) as a broad curve with peak maximum at ca.

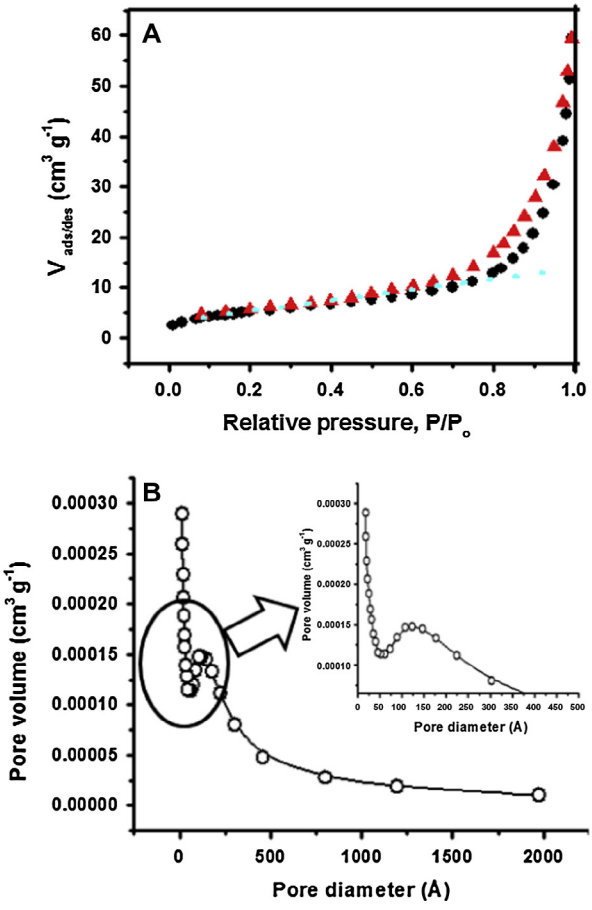

Figure 1 Plot of relative pressure versus volume of adsorption/desorption of CDC@500 °C (A) pore size distribution of CDC@500 °C (B).

12.5 nm. The pore volume decreases to a minimum for a pore size of 5 nm, once again increases to a maximum at 12.5 nm and then decreases further. The average pore diameter after BJH adsorption and desorption was observed to be 19.2 nm and 15.4 nm, respectively.

Iodine number evaluates the surface area of carbons associated with pores larger than 1 nm (Patnukao and Pavasant, 2008) and gives an indication of adsorption capacity in micropores. The iodine number of CDC@500 °C was measured to be 912 mg g^{-1} with the specific surface area of 18.3 m^2 g^{-1}.

3.1.3. Scanning electron microscopy

Scanning electron micrographs (Fig. 2) show a disorganized structure of carbons especially CDC@500 °C and CDC@700 °C. The presence of SiO_2 and other inorganic compounds precipitates along with the ash are observed as sharp edged crystallites and ash – like fine particles. The particles appear with high heterogeneity in shapes but the images of CDC@700 °C appear with high degree of rupture leading to fine along with huge particles with the formation of alkali metal oxides, alkaline metal carbonates and silica. The EDS analysis of non-modified CDC shows that it contains a lot of elements (with % weight) besides the expected C (67.00%) and O (24.86%): Si (3.18%), Ca (1.69%), P (0.75%), K (0.67%), Na (0.62%), Mg (0.56%), Al (0.34%) and Cl (0.32%). The EDS analysis shows the increased Si (as SiO_2) content from 3.4% to 13% (by weight) for non-modified CDC when the carbonization temperature increases. This occurs due to the decrease in carbon mass which there by increased the mass of silica to the total mass of carbons on increasing the temperature from 300 °C to 700 °C. As a consequence of thermo-chemical reactions which take place during carbonization, the separation of metal compounds as oxides, carbonates and chlorides from the carbon surface is well witnessed from the EDS analysis and reveals the existence of K, Ca and Mg as main elements and Fe in minor amounts. The thermal destruction of particles accompanied with the precipitation of inorganic compounds was well documented from the images captured for CDC@500 °C and CDC@700 °C. The SEM images of CDC@300 °C remain with little distortion and contain bigger particles with higher degree of heterogeneity. However, these images appear to have well developed structures containing cracks and voids and may be trapped with acidic oxides (phosphorus and nitrogen oxides), which on hydrolysis give a solution of acidic nature.

3.1.4. pH_{PZC}

The pH_{PZC} of cattle dung (7.80) and CDC is represented in Fig. S1. It shows that the pH_{PZC} for CDC@500 °C and CDC@700 °C was 9.30 and 9.61, respectively. The increased pH_{PZC} toward basic medium is evidently associated with the formation of inorganic compounds during carbonization. This is in agreement with the research studies which corroborated the separation of alkali salts from the organic matrix after pyrolysis of bio-materials (Lu et al., 2012). Interestingly, the pH_{PZC} for the raw cattle dung (prepared as slurry) was measured to be 7.80. This cattle dung on carbonization releases various volatile gases in addition to oxides of carbon, hydrides of nitrogen and oxygen. As a consequence of carbonization at 300 °C and due to thermo-chemical reactions, the pH_{PZC} of yielded CDC descends to 6.25.

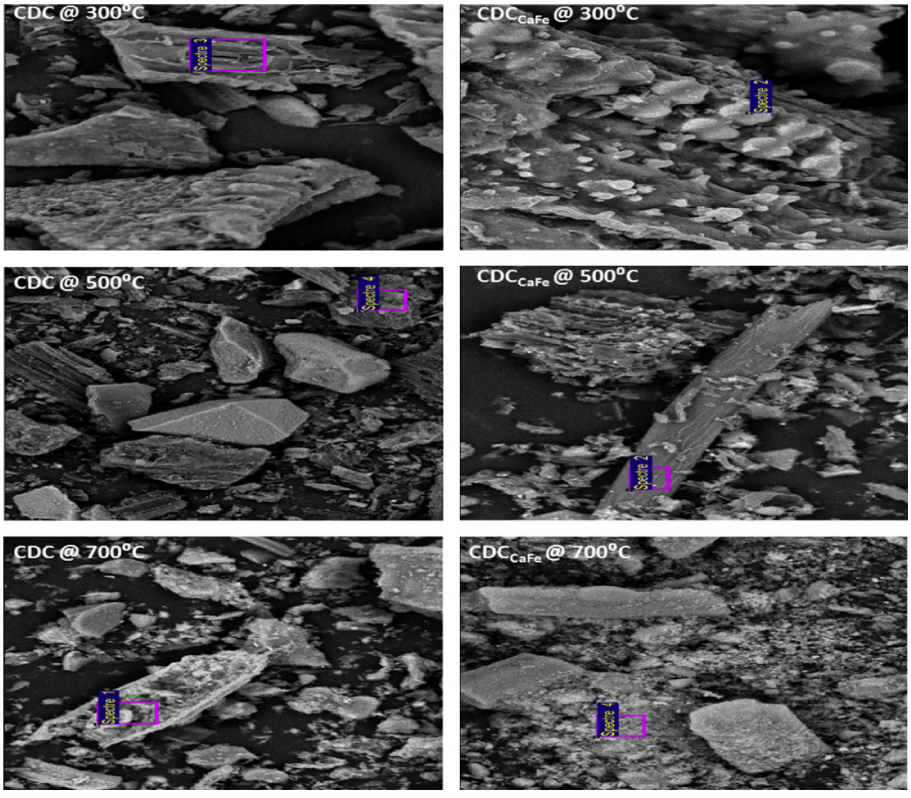

Figure 2 Scanning electron micrographs for CDCs and ICDCs (CDC_{CaFe}).

3.1.5. X-ray diffraction

The powder X-ray diffraction patterns of non-modified CDC show characteristic peaks particularly with the two main diffractions around 2θ values equal to 21° and 26.5°. These rays substantiate the presence of SiO_2 in CDC and the nature of CDC becomes quasi – amorphous. SiO_2 crystallites are attributed to quartz particles by comparison of intensities of peaks around 21° and 26.5° in Fig. 3A–C.

3.1.6. Infrared spectroscopy

The FTIR characterization (Fig. S2) for CDC@500 °C is as follows. The IR absorption bands at 1535 cm^{-1} and 1550 cm^{-1} correspond to the double bond (C═C) vibrations in an aromatic system and the highly conjugated C─O stretching vibrations respectively (Pakula et al., 2007). The absorption bands at 2347 cm^{-1} and 2926 cm^{-1} are associated with the symmetric and asymmetric stretching vibrations of alkyne (─C≡C─) and methylene (─CH_2─), respectively. The bending vibration for ─CH_2─ group was observed at 1379 cm^{-1}. A peak at 1398 cm^{-1} is associated with the carbonate which ascertains the presence of inorganic groups present on the carbon matrix along with the superposition of various oxides in the assignment range 400–800 cm^{-1}. A slightly broad peak at 1597 cm^{-1} indicated the presence of ═CO stretching vibration and a sharp peak at 1101 cm^{-1} was associated with the Si─O

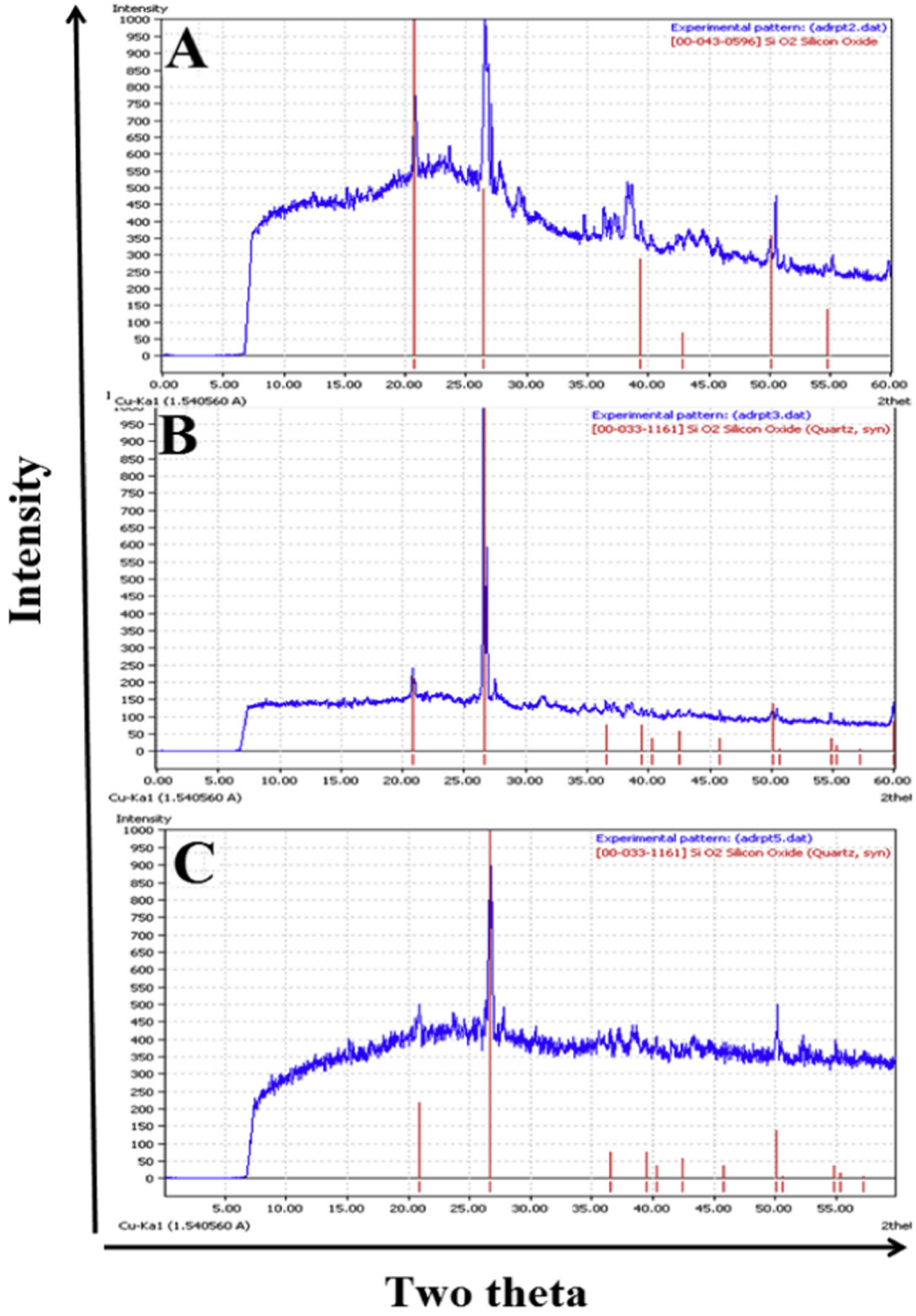

Figure 3 X-ray diffraction profiles of CDC@500 °C (A) CDC_{CaFe}@500 °C (B) and CDC@700 °C (C).

bond of the silica framework which is further substantiated from XRD study.

3.1.7. Surface acidity/basicity

The acid–base character of carbons is shown in Table 3 from Boehm titration. The acidity decreases and the basicity increases with increasing the carbonization temperature. The notable observation is that carbons exhibit a great basicity which reaches 4.95 mmol g^{-1} for CDC@700 °C. This result may be attributed to the inorganic content of carbons which allows the trapping of CO_2 during the carbonization and the formation of carbonate compounds.

3.1.8. Effect of CaFe impregnation

The effect of impregnation of cattle dung with calcium and ferric salts may be the result of two reactions. Firstly, the impregnation solution can act as a washing treatment with an acid solution which is able to change the acid/base character of carbons. Secondly, the remaining Ca and Fe compounds after carbonization are known as improving elements in defluoridation adsorbents (Tchomgui-Kamga et al., 2010a,b).

The CaFe impregnation did not modify the SEM structure of the adsorbents. All the carbons showed the presence of Fe as new element. Despite the impregnation of cattle dung with Ca/Fe solution the atomic percentage of Fe was always higher than that of Ca. This observation may be the result of a washing effect during the impregnation process. Ca content in ICDC was not higher than in corresponding CDC. The Cl atomic content was lower than that of Ca or Fe, showing that this element escaped during the carbonization or did not enter into the cattle dung during the impregnation. The washing effect was observed on the Si content which was found at 5–8.5% by weight for ICDC instead of 3.4–13% by weight for CDC. The acid effect of the washing was observed at two points. First, the pH_{PZC} notably decreases at 5.5, 7.9 and 7.8 for CDC_{CaFe}@300 °C, CDC_{CaFe}@500 °C and CDC_{CaFe}@700 °C, respectively, instead of 6.25, 9.3 and 9.6 for the non-modified CDC (Fig. S1). The second point is about the acid/base character of the ICDCs which exhibit a clear decrease of the base content when the carbonization temperature was at 500 °C and 700 °C (Table 3).

It is conspicuous that the basic nature for non-modified CDC is greater than that of ICDC. The fall in the pH value may be attributed to the thermo-chemical reactions involved during the carbonization process between metal (Ca and Fe) chlorides and surface precipitated compounds such as metal oxides and metal carbonates on the CDC matrix.

Table 3 Surface acidity and basicity of CDCs and ICDCs.

Sample	Acidic (mmol g^{-1})	Basic (mmol g^{-1})
CDC@300 °C	1.50	1.69
CDC@500 °C	0.76	4.21
CDC@700 °C	0.44	4.95
CDC_{CaFe}@300 °C	2.02	2.22
CDC_{CaFe}@500 °C	0.46	1.62
CDC_{CaFe}@700 °C	0.76	2.09

3.2. Defluoridation studies

3.2.1. Initial optimization studies and effect of pH

The influence of pH during the sorption of fluoride onto carbons plays a significant role in the defluoridation process. All the synthesized carbons were investigated for their fluoride uptake capacity using the dose of 2 g L^{-1} having the initial fluoride concentration of 2 mg L^{-1}. The initial pH of the fluoride solution was 6.95 ± 0.05. The fluoride sorption potential of carbons is in the descending order as follows, with their fluoride uptake capacities in brackets:

$$\text{CDC@500 °C}\ (15\ \text{mg g}^{-1}) > \text{CDC}_{\text{CaFe}}\text{@500 °C}\ (9\ \text{mg g}^{-1}) > \text{CDC}_{\text{CaFe}}\text{@300 °C}\ (7\ \text{mg g}^{-1}) > \text{CDC@300 °C}\ (4\ \text{mg g}^{-1}) \approx \text{CDC}_{\text{CaFe}}\text{@700 °C}\ (4\ \text{mg g}^{-1}) > \text{CDC@700 °C}\ (3\ \text{mg g}^{-1})$$

With justification, CDC@500 °C was chosen for other defluoridation experiments with an objective of defluoridation efficiency as a function of contact time, pH, dose, temperature and interfering anionic competitors. The optimized contact time at which the equilibrium established between the two phases of fluorides ($F_{adsorbate}$ and $F_{aqueous}$) was at 40 min. Based on the above optimized time and dose conditions, the influence of pH on fluoride sorption onto CDC@500 °C and the alteration in the solution pH levels were explored as shown in Fig. 4A. The fluoride removal efficiency was directly proportional to pH up to 7.53 but becomes inversely proportional thereafter till the pH value of 11.53. The highest removal was influenced at the pH of 7.53 and the lowest removal took place at strongly acidic and basic conditions with the pH values of 2.08 and 11.53 respectively. The fluoride removal at acidic conditions was minimum due to the formation of hydrofluoric acid (HF, pK_a = 3.18). The pH_{PZC} of CDC@500 °C was 9.09 and this basic shift is associated with the presence of inorganic oxides and carbonates on the surface of the carbon matrix. On accounting the fact that the pH < pH_{PZC} develops the carbon surface with positive charges but when the pH value approaches 9.09 (pH_{PZC}), the fluoride sorption decreases drastically as it could be observed in the present study. The sharp decline in fluoride removal after the pH of 7.99 is due to the significant decrease in the concentration of the protonated surface sites or fluoride binding sites on increasing the pH value. In addition, at basic conditions the arising competition between fluoride and hydroxide groups (almost similar size and mono-negative charge) for the same surface active site is most likely and hence the declining fluoride sorption onto the carbon is accounted. Similar conclusions were obtained for carbonaceous adsorbents (Sivasankar et al., 2011, 2013).

Mattson and Mark (1971) interpreted that the carbon (termed H type) activated at higher temperatures (600–1000 °C) develops basic surface sites and increases the pH value of neutral or acidic solutions. This type of carbon is capable of reacting with acids and develops a positive zeta potential. Based on this fact, it may also be accounted that the protonation of basic functions on the carbon matrix by H_3O^+ ions at lower pH conditions is disfavored due to the reaction between the basic surface sites and H^+ ions. Accordingly, the final pH of the fluoride solution is increased after the fluoride sorption (Fig. 4A). Daifullah et al. (2007) claimed a two-step ligand exchange mechanism for fluoride adsorption. This study inferred that the pH of the aqueous fluoride solution increased

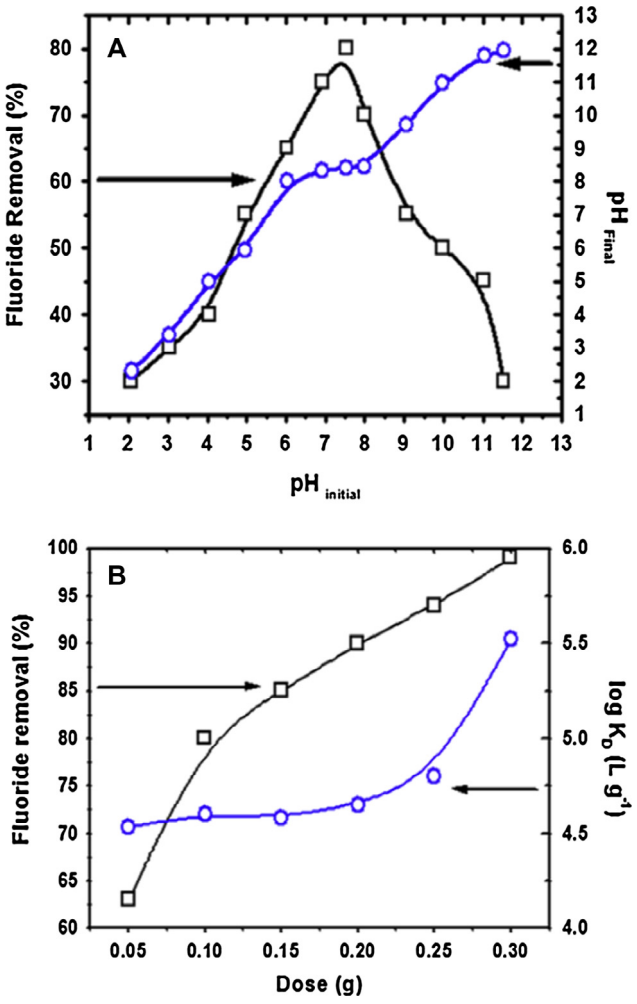

Figure 4 Fluoride removal as a function of pH for 0.01 g of CDC@500 °C (A) and CDC@500 °C dose at pH 7.50 ± 0.05 (B) (volume of solution 0.05 L).

after the fluoride sorption due to the lowering of H_3O^+ concentration because of its tendency to protonate internal functions of the carbonaceous material.

3.2.2. Effect of CDC@500 °C dose

The fluoride removal by CDC@500 °C was calculated in the range 63–99%. The removal difference was 17% on increasing the adsorbent concentration from 1.0 g L^{-1} to 2.0 g L^{-1}. Further increase in the adsorbent concentration from 2.0 g L^{-1} to 6.0 g L^{-1} did not achieve any appreciable sorption ability. The sorption of fluoride onto CDC@500 °C was almost constant when the adsorbent concentration exceeded 6.0 g L^{-1}. This was due to the overlapping of active sites at higher dosage as well as the decrease in the effective surface area resulting in the conglomeration of exchanger particles (Killedar and Bhargava, 1993).

The fluoride uptake increase with respect to the increase in dose of CDC@500 °C was attributed to the higher availability of surface pore volume of the carbon materials. Although the percentage of fluoride removal was found to increase with respect to the increase in adsorbent dose, the fluoride sorption capacity (mg g^{-1}) for a particular adsorbent approaches the descending trend due to the following facts:

- Better utilization of active sites at lower doses but the sites become superfluous at higher doses for the limited quantity of fluoride.
- The operation of driving forces responsible for fluoride sorption becomes negligible despite the usage of high doses.

A distribution coefficient K_D (Murray and Stumm, 1988) is one which reflects the binding ability of the surface of an adsorbent and depends on the pH of the solution and the surface of the adsorbent. K_D can be calculated with Eq. (13) where C_s is the concentration of fluoride on the solid particles (mg kg^{-1}) and C_w is the equilibrium concentration in solution (mg L^{-1}).

$$K_D = C_s/C_w(\text{L kg}^{-1}) \tag{13}$$

Fig. 4B shows that the K_D value increases as the dose of CDC@500 °C increases at the constant pH and it implies the increasing surface heterogeneity of the adsorbent as reported by earlier researchers (Chen et al., 2011).

3.2.3. Adsorption kinetics

The study of adsorption kinetics is significant because it provides valuable insight into the reaction pathway and fluoride sorption mechanism. The sorption mechanism depends on the physical and chemical characteristics of the adsorbent and also on the mass-transfer process.

The dynamics of fluoride sorption onto CDC@500 °C at an optimized pH (7.53) and adsorbent concentration (2 g L^{-1}) with respect to different initial fluoride concentrations (2–8 mg L^{-1}) and temperatures (298 K, 308 K and 318 K) was validated using kinetic models such as pseudo-first-order, pseudo-second-order, intra-particle diffusion and Elovich models. The figured parameters of the kinetic models are represented in Table 4. Based on pseudo-first-order and pseudo-second-order models, it is possible to elucidate the mechanism of adsorption and potential rate controlling steps of fluoride sorption onto CDC@500 °C.

Pseudo-first-order model is a simple adsorption kinetic model, suggested by Lagergren (1898) and further referred by Ho et al., and is unable to apply throughout the range of tested contact time. The regression values (Table 4) indicated the applicability of pseudo-first-order and the range was 0.833–0.959, 0.967–0.971 and 0.936–0.967 respectively for 298 K, 308 K and 318 K.

According to pseudo-second-order kinetics, rate of adsorption is directly proportional to the number of active sites on the adsorbent surface. The compliance of the pseudo-second-order model seems appreciable and the most of the regression coefficients are $\geqslant$0.98. Based on the regression values, it may be ascertained that the pseudo-second-order was more validated than that of the pseudo-first-order model as observed by earlier researchers (Yadhav et al., 2013).

It is inferred from the Weber–Morris intra-particle diffusion plot that the initial curved portion reflects the film or boundary layer diffusion effect and the subsequent linear portion (plateau) is pertinent to the intra-particle diffusion effect (Ghoari and Pant, 2005). The graphical plots deviate from passing through the origin and the deviation may be

Table 4 Parametric data of kinetic models for fluoride sorption onto CDC@500 °C at different temperatures.

$[F]_o$	Pseudo-first-order			Pseudo-second-order				Elovich			Intra-particle diffusion		
	k_1 ($\times 10^{-2}$)	q_e	R^2	k_2 ($\times 10^{-2}$)	q_e	h	R^2	A	B	R^2	K_i	C	R^2
Temperature: 298 K													
2	2.42	10.07	0.833	6.57	1.87	0.23	0.916	8.1	0.298	0.776	1.96	4.11	0.870
3	3.05	7.67	0.951	16.10	2.53	1.03	0.994	97.0	0.387	0.904	1.47	15.52	0.966
4	3.46	16.83	0.947	6.69	3.73	0.93	0.989	73.6	0.183	0.936	3.09	16.53	0.984
5	2.78	17.62	0.921	5.33	3.86	0.79	0.977	44.1	0.163	0.903	3.49	14.67	0.956
6	3.71	30.48	0.959	3.31	5.52	1.01	0.985	41.7	0.105	0.921	5.37	18.07	0.969
7	3.49	33.65	0.947	2.78	6.21	1.07	0.981	40.9	0.092	0.936	6.18	19.06	0.984
8	3.59	44.26	0.838	1.95	7.09	0.98	0.959	32.3	0.076	0.881	7.51	17.02	0.948
Temperature: 308 K													
2	2.69	4.09	0.967	28.50	1.08	0.33	0.992	48.1	0.718	0.938	0.79	5.53	0.983
3	2.82	8.18	0.967	7.12	1.29	0.12	0.956	2.7	0.359	0.937	1.57	1.05	0.981
4	3.12	8.18	0.967	14.25	2.15	0.66	0.992	96.3	0.359	0.939	1.57	11.05	0.983
5	3.19	12.27	0.967	8.08	2.56	0.53	0.985	27.0	0.239	0.945	2.36	9.58	0.988
6	3.29	12.53	0.971	9.78	3.52	1.21	0.994	295.5	0.239	0.940	2.36	19.58	0.983
7	3.48	16.37	0.967	6.50	3.73	0.91	0.988	65.4	0.180	0.948	3.14	16.10	0.989
8	3.94	16.37	0.967	7.43	4.69	1.64	0.993	394.3	0.180	0.937	3.14	26.10	0.983
Temperature: 318 K													
2	3.69	5.47	0.936	18.54	1.02	0.19	0.982	9.1	0.588	0.906	0.97	3.56	0.964
3	3.62	10.94	0.936	9.40	3.55	0.62	0.985	12.0	0.294	0.906	1.57	1.05	0.983
4	3.46	8.18	0.967	13.46	1.96	0.52	0.990	46.9	0.359	0.937	1.57	9.05	0.985
5	3.35	12.27	0.967	7.14	2.30	0.38	0.979	13.2	0.239	0.937	2.36	6.58	0.983
6	3.16	12.27	0.967	9.51	3.23	0.99	0.992	144.1	0.239	0.937	2.36	16.58	0.982
7	2.81	16.37	0.967	5.93	3.37	0.67	0.984	32.0	0.180	0.939	3.14	12.10	0.987
8	2.53	16.37	0.967	7.10	4.31	1.32	0.992	192.2	0.180	0.937	3.14	22.10	0.983

caused due to the difference between the rate of mass transfer in the initial and final stages of fluoride sorption and the complex mechanism which involves the contribution of both the surface adsorption and intra-particle diffusion to the rate determining step (Ghoari and Pant, 2005). The thickness of boundary layer as determined from the intercept value C is inversely proportional to the external mass transfer. The value of C seems to be very sensitive with respect to the change in initial fluoride concentration and temperature. The regression values indicate the intra-particle diffusion model fit with the fluoride sorption dynamics.

Elovich model is one among the useful kinetic models for describing chemisorption. The calculated values of initial adsorption rate (A) and constant of desorption (B) with corresponding regression coefficients indicate that the Elovich model fits fairly well with the present system on fluoride sorption onto CDC@500 °C.

3.2.4. Adsorption isotherms

Equilibrium data can be analyzed using well known adsorption isotherms, which provide the basis for the design of adsorption systems. The most widely adopted isotherm equations for modeling of the experimental data are Langmuir and Freundlich equations. The former is being purely empirical and the later assumes that maximum sorption occurs when the surface is covered by the adsorbate. The details of equations are presented in Table 1.

The Freundlich model (Eq. (7)) is based on the sorption which takes place on a heterogeneous phase.

The degree of non-linearity between fluoride in solution and CDC@500C is indicated by the values of 'n'. When $n = 1$, then sorption of fluoride is linear. The values of $1/n$ predict the nature of sorption to be whether normal ($1/n < 1$) or cooperative ($1/n > 1$) and also reported to represent a joint measure of both the relative magnitude and diversity of energies associated with a particular sorption process (Freundlich, 1906). In the present system, a cooperative or S-type or solvent affinity-type isotherm is associated where the marginal sorption energy increases with increasing surface concentration (Farrell and Reinhard, 1994). It can also be interpreted with strong adsorption of solvent, strong intermolecular attraction within the adsorbed layers, penetration of the solute (fluoride) in the adsorbent (CDC@500C) and mono-functional nature of the fluoride adsorbate. The fluoride sorption capacity (K_F) decreases from 36.14 mg g^{-1} to 6.43 mg g^{-1} with respect to the increase in the temperature from 298 K to 318 K. The decrease in the fluoride sorption capacity was around 5.62 times for the gradation of 20 K. In support of this decrease in fluoride sorption, the heterogeneity of surface ($1/n$) was accordingly decreased for CDC@500 °C on increasing the temperature from 298 K to 318 K. The value of $1/n$ was found to ascend from 0.69 to 1.15 with 1.67 folds on increasing the temperature. It is reasonable to remember that $1/n$ value tends to increase with the increase in temperature, according to theory of dilution. The decreasing trend in fluoride sorption to the increasing temperature may be associated with the thickness of the boundary layer at which the molecular escape into the solution phase is facilitated especially at high temperatures. The present observation is in agreement with early researchers (Daifullah et al., 2007). Even though, the agreeable fit (R^2 = 0.912–0.977) of experimental data, Freundlich model does not provide a conclusive evidence for

the fluoride sorption mechanism, it provides an indirect evidence for site heterogeneity and/or surface heterogeneity. On the basis of energy possessed by each affinity site, the sorption of fluoride takes place in preference primarily to the stronger binding sites followed by other sites in the order of decreasing energy till the sorption of fluoride is complete.

According to Langmuir model (Eq. (6)), the amount of fluoride adsorbed onto CDC@500 °C was decreased from 111.11 mg g^{-1} to 66.67 mg g^{-1} with the corresponding Langmuir isotherm constants of 0.500 L mg^{-1} and 0.081 L mg^{-1} respectively. The feasibility of Langmuir isotherm can be expressed in terms of a dimensionless constant or equilibrium parameter, R_L which is equal to $[1/(1 + bC_0)]$. The data of dimensionless constant were found between 0 and 1 and thus the favorable sorption of fluoride could be inferred.

Dubinin–Radushkevich (D–R) isotherm is more general than Langmuir isotherm owing to its disagreement for a homogenous surface or a constant adsorption potential. Using D–R equations (Eqs. (8)–(10)) with reference to the present system, the constant β gives the free energy, E (kJ mol^{-1}) for the transfer of 1 mol of fluoride from infinity to the surface of CDC@500 °C and can be computed using the relationship. The magnitude of E is helpful in understanding the nature of fluoride sorption. The recorded values of E (Table 5) decreased from 7.91 kJ mol^{-1} to 7.02 kJ mol^{-1} with the increase in temperature from 298 K to 318 K. It is very apparent that $E < 8$ kJ mol^{-1} ascertained the nature of fluoride sorption under the governance of physical forces (Swain et al., 2010).

3.2.5. Effect of temperature and evaluation of thermodynamic parameters

The effect of temperature on fluoride sorption onto CDC@500 °C was studied at 298 K, 308 K and 318 K for the initial fluoride concentration of 2–8 mg L^{-1} at optimized pH and adsorbent concentration. The related thermodynamic parameters such as ΔG, ΔH and ΔS were calculated using Eqs. (11) and (12) (Table 1). ΔH represents the difference in binding energies between the sorbent and sorbate and, between the solvent and solute. Thus, sorption may occur as the result of two types of forces: enthalpy-related and entropy-related forces. In the case of hydrophilic bonding, the enthalpy related forces are greater due to the additional contribution of electrostatic interactions. The isosteric enthalpy of fluoride sorption between −43.65 kJ mol^{-1} and −95.18 kJ mol^{-1} in the present system was recorded as an indicative of exothermic process or exothermic binding reaction. According to Giles classification (Vinod and Anirudhan, 2001), the present fluoride sorption supports the subgroup III with temperature range 10–40 °C at which the saturation of CDC@500 °C surface seems to be reached and hence the optimal temperature of fluoride sorption could be investigated within this range. Sorption of a chemical on a solid adsorbent occurs when the free energy of the sorptive exchange is negative. The negative ΔG values indicate the spontaneous nature of fluoride sorption and decrease from 298 K to 318 K. As the free energy change of the present fluoride sorption was evaluated in the range 0–20 kJ mol^{-1}, the governance of bonding by physical forces may be suggested to be the dominant mechanism. The trend in the feasibility of fluoride sorption descends from 298 K to 318 K as shown in Table 6.

Lower sorption of fluoride at higher temperature may be associated with the dependence of sorption coefficients and solubility on temperature. Hence the measured effect of temperature on sorption isotherms is the result of combined sorption and solubility contributions. The decreasing sorption at higher temperature (Fig. S3) may be associated with weak interactive forces between CDC@500 °C and fluoride by suggesting physisorption. The negative entropy change during fluoride sorption at all temperatures signifies orderliness of the system and enthalpy driven. The entropy change is consistent with the restricted mobility of adsorbed fluoride as compared to that in solution.

3.2.6. Desorption studies

Treatment by sorption technology is economical and advantageous if the exhausted adsorbent material can be regenerated. Fluoride desorption by NaOH solutions is presented in Fig. 5A for CDC@500 °C. Fluoride desorption using 0.05 M NaOH solution was achievable up to 100% for the initial fluoride concentration of 2 mg L^{-1}. But, desorption percentage was found to be inversely proportional to the initial fluoride concentration. The percentage of fluoride desorption was reduced around 50% for the initial fluoride concentrations of 4 mg L^{-1} and 5 mg L^{-1}. From this 50% of desorption, the percentage further decreases to about 26% for the initial fluoride concentration of 8 mg L^{-1}. Using 0.1 M NaOH solution, 100% of desorption was achieved up to 4 mg L^{-1}. But, desorption of fluoride was found to decrease and comparatively high (~2 folds) as that of 0.05 M NaOH solution for the initial fluoride concentrations from 4 mg L^{-1} to 8 mg L^{-1}. Desorption of fluoride was 100% for all the initial fluoride concentrations using 0.2 M NaOH solution. From the above results, it is wise to consider 0.05 M NaOH for desorption of fluoride loaded CDC@500 °C using 2 mg L^{-1} and 3 mg L^{-1} of initial fluoride concentrations. But 0.1 M NaOH solution is the commendable choice for desorption of fluoride loaded material using 3–5 mg L^{-1} of initial fluoride concentration. The fluoride loaded CDC@500 °C with 6–8 mg L^{-1} may be opted with 0.2 M NaOH solution for desorption experiments.

Table 5 Freundlich and Langmuir isotherm constants for fluoride adsorption onto CDC@500 °C.

Temperature (K)	Freundlich				Langmuir			DKR
	$1/n$	n	K_F	R^2	Q°	b	R^2	E (kJ mol^{-1})
298	0.69	1.45	36.14	0.912	111.11	0.500	0.767	7.91
308	1.12	0.89	8.18	0.947	83.83	0.084	0.781	7.07
318	1.15	0.87	6.43	0.977	66.67	0.081	0.771	7.02

Table 6 Thermodynamic data on fluoride sorption dynamics onto CDC@500 °C.

F (mg L^{-1})	ΔH (kJ mol^{-1})	ΔS (kJ mol^{-1})	ΔG (kJ mol^{-1})		
			298 K	308 K	318 K
2	−62.99	−0.182	−9.139	−5.896	−5.557
3	−95.18	−0.290	−9.139	−4.121	−3.413
4	−76.86	−0.226	−10.002	−5.896	−5.557
5	−49.65	−0.141	−7.804	−5.485	−5.015
6	−55.01	−0.155	−9.139	−6.410	−6.087
7	−59.67	−0.172	−8.718	−5.749	−5.327
8	−43.56	−0.118	−8.427	−6.410	−6.088

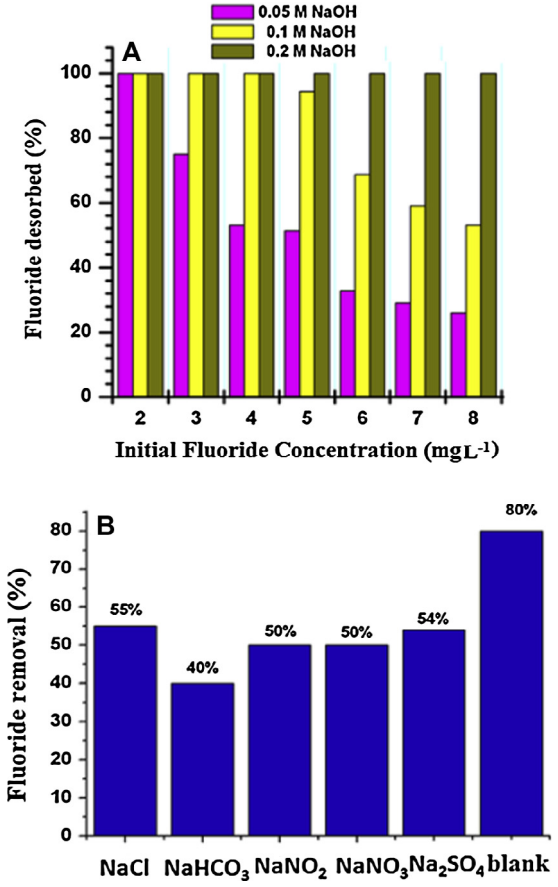

Figure 5 Desorption of fluoride at different initial concentrations (A). Interference of co-ions (B) at the concentration 1 g L^{-1} of CDC@500 °C.

3.2.7. Competition of other anions against fluoride

The present section discusses on the fluoride removal by CDC@500 °C as a function of co-ions interference which include sodium salt of chloride, hydrogen carbonate, nitrite, nitrate and sulfate at 0.5 M concentration. The behavior of fluoride sorption in the environment of the other (inner and outer sphere) complex forming ions is explored. The 80% efficiency of fluoride removal was reduced to 40%, 50%, 54% and 55% respectively when HCO_3^-, NO_3^- (and NO_2^-), SO_4^{2-} and Cl^- ions accompanied the fluoride ion in the binary interference system (Fig. 5B). The low affinity ligands such as NO_3^-, NO_2^- and Cl^- follow the sorption mechanism via the formation of weaker bonds with the active sites at the Helmholtz plane through outer-sphere complexation. Hence lesser inhibitory effect as compared to other anions was experienced. Sulfate ions form partial outer- and inner-sphere complexes and there are two possible causes corroborated for the sulfate hindrance in fluoride sorption. One is the competition between sulfate and fluoride for the same sorption site since the former is partially inner-sphere complex forming species. The other is the increasing coulombic repulsive forces due to the divalent sulfate ion (in solution) could lessen the probability of fluoride interaction with the active sites. Hydrogen carbonate, a pH buffering agent could raise and buffer the pH of the solution leading to the decreased uptake of fluoride by the adsorbents. The greater interference of HCO_3^- is studied to be more dominant than the other species as referred in the literature (Msagati et al., 2014).

Table 7 Comparative sorption capacity figures of other carbonaceous adsorbents with CDC@500 °C.

S. no.	Carbonaceous material	Adsorption capacity (mg g^{-1})	Reference
01.	Carbon slurry	4.86	Tchomgui-kamga et al. (2010a,b)
02.	Pine wood biochar	7.66 & 9.77	Mohan et al. (2012)
03.	Lignite	13.8	Msagati et al. (2014)
04.	Restructured lignite	15.8	Msagati et al. (2014)
05.	Carbonized cattle dung (CDC) CDC@500 °C	15.0	Present study
06.	*Tamarindus Indica* Fruit Shell Carbon (*TIFSC*)	19.66	Sivasankar et al. (2012a,b)

3.2.8. Comparison of carbonaceous fluoride adsorbents

A comparison has been made between carbons synthesized in this work and previously reported carbonaceous adsorbents for fluoride removal. There are two kinds of carbon adsorbents. Some of them arise from carbonization of natural biomass and others are modified carbons which are obtained by carbonization of impregnated biomass. The results for some unmodified carbons are presented in Table 7. As can be seen

from these results, CDC@500 °C is as efficient as lignite materials in terms of defluoridation capacity.

4. Conclusions

In the present study, new efficient fluoride adsorbents were prepared by carbonization of cattle dung, with a previous impregnation by $CaCl_2$ and $FeCl_3$ solutions and without any impregnation leading to carbon materials denoted ICDC and CDC, respectively. These adsorbents and particularly CDC are easily available in rural countries. CDC adsorbents have shown a good efficiency in fluoride removal from aqueous solutions. The carbonization used during their preparations is a sanitization process which allows the uses of these adsorbents in drinking water. The main conclusions drawn from the present study are as follows:

- As for previous examples of carbons arising from carbonization of biomass materials, the impregnation with $CaCl_2$ and $FeCl_3$ solutions did not increase the defluoridation efficiency of the ICDC by comparison with CDC.
- CDC adsorbents were mainly basic. The basic character was less marked for modified adsorbents ICDC.
- The most efficient fluoride adsorbent was CDC@500 °C. For this adsorbent the adsorption kinetic followed the pseudo-second-order model which indicates that fluoride removal could be a chemisorptions process. The adsorption isotherm was better fitted by the Freundlich model.
- An optimum fluoride removal by CDC@500 °C was observed at pH 7–8.
- A full fluoride adsorption study was performed for CDC@500 °C. This study includes the effect of coexisting ions and regeneration experiments by washing F-loaded adsorbents with NaOH solutions.

Acknowledgments

The authors thank the Principals and managements of Pachaiyappa's College, Chennai – 600 030, Tamil Nadu, India, and Thiagarajar College of Engineering (Autonomous), Madurai – 625 015, Tamil Nadu, India. The corresponding author is greatly indebted to Dr. R. Prabhaakaran, former President and present Trustee, Pachaiyappa's Board Trust, Chennai – 600 030, for his constant support and encouragement to all his research endeavors.

Appendix A. Supplementary material

Supplementary data associated with this article can be found, in the online version, at http://dx.doi.org/10.1016/j.arabjc.2015.06.028.

References

Aggarwal, G.C., Singh, N.T., 1984. Energy and economic returns from cattle dung as manure and fuel. Energy 9, 87–90.
Aharoni, C., Tompkins, F.C., 1970. Kinetics of Adsorption and Desorption and the Elovich Equation. Advance in Catalysis and Related Subjects. Academic Press, New York.
Amini, M., Mueller, K., Abbaspour, K.C., Rosenberg, T., Afyuni, M., Møller, K.N., Sarr, M., Johnson, C.A., 2008. Statistical modeling of global geogenic fluoride contamination in groundwaters. Environ. Sci. Technol. 42, 3662–3668.
Andezhath, S.K., Ghosh, G., 2000. Fluorosis management in India: the impact due to networking between health and rural drinking water supply agencies. Interdisciplinary perspectives on drinking water risk assessment and management. IAHS Publication 260, 159–165.
Bhatnagar, A., Sillanpää, M., 2010. Utilization of agro-industrial and municipal waste materials as potential adsorbents for water treatment – a review. Chem. Eng. J. 157, 277–296.
Bhattacharya, D., Yu, J.S., 2014. Activated carbon made from cow dung as electrode material for electrochemical double layer capacitor. J. Power Sources 262, 224–231.
Boehm, H.P., 1994. Some aspects of the surface chemistry of carbon blacks and other carbons. Carbon 32, 759–769.
Brouwer, I.D., Bruin, A.D., Dirks, O.B., Hautvast, J.G.A.J., 1988. Unsuitability of World Health Organization guidelines for fluoride concentration in drinking water in Senegal. Lancet 331, 223–225.
Chen, N., Zhang, Z., Feng, C., Zhu, D., Yang, Y., Sugiura, N., 2011. Preparation and characterization of porous granular ceramic containing dispersed aluminum and iron oxides as adsorbents for fluoride removal from aqueous solution. J. Hazard. Mater. 186, 863–868.
Chidambaram, S., Manikandan, S., Ramanathan, A.L., Prasanna, M.V., Thivya, C., Karmegam, U., Karmegam, U., Thilagavathi, R., Rajkumar, K., 2013. A study on the defluoridation in water by using natural soil. Appl. Water Sci. 3, 741–751.
Daifullah, A.A.M., Yakout, S.M., Elreefy, S.A., 2007. Adsorption of fluoride in aqueous solutions using $KMnO_4$-modified activated carbon derived from steam pyrolysis of rice straw. J. Hazard. Mater. 147, 633–643.
Das, D.D., Mahapatra, R., Pradhan, J., Das, S.N., Thakur, R.S., 2000. Removal of Cr(VI) from aqueous solution using activated cow dung carbon. J. Colloid. Interface Sci. 232, 235–240.
Demiral, H., Demiral, I., 2008. Surface properties of activated carbon prepared from wastes. Surf. Interface Anal. 40, 612–615.
Demiral, H., Demiral, I., Karabacakoglu, B., Tumsek, F., 2011. Production of activated carbon from olive bagasse by physical activation. Chem. Eng. Res. Des. 89, 206–213.
Dias, J.M., Alvim-Ferraz, M.C.M., Almeida, M.F., Rivera-Utrilla, J., Sanchez-Polo, M., 2007. Waste materials for activated carbon preparation and its use in aqueous- phase treatment: a review. J. Environ. Manage. 85, 833–846.
Dubinin, M.M., Radushkevich, L.V., 1947. The equation of the characteristic curve of the activated charcoal. Proc. Acad. Sci. USSR. Phys. Chem. Sect. 55, 331–333.
Elaigwu, S.E., Usman, L.A., Awolola, G.V., Adebayo, G.B., Ajayi, R.M.K., 2009. Adsorption of Pb(II) from aqueous solution by activated carbon prepared from cow dung. Adv. Natural Appl. Sci. 3, 442–446.
Erdal, S., Buchanan, S.N., 2005. A quantitative look at fluorosis, fluoride exposure, and intake in children using a health risk assessment approach. Environ. Health Perspect. 113, 111–117.
Farrell, J., Reinhard, M., 1994. Desorption of halogenated organics from model solids, sediments and soil under unsaturated conditions 2. Kinetics. Environ. Sci. Technol. 28, 63–72.
Freundlich, H.M.F., 1906. Uber die adsorption in losungen. Z. Phys. Chem. 57A, 385–470.
Ghoari, S., Pant, K.K., 2005. Equilibrium, kinetics and breakthrough studies for adsorption of fluoride on activated alumina. Sep. Purif. Technol. 42, 265–271.
Grandjean, P., Landrigan, P.J., 2006. Developmental neurotoxocity of industrial chemicals. Lancet 368, 2167–2178.
Ho, Y.S., Wase, D.A.J., Forster, C.F., 1996. Kinetic studies of competitive heavy metal adsorption by Sphagnum moss peat. Environ. Technol. 17, 71–77.

Hussain, J., Sharma, K.C., Hussain, I., 2004. Fluoride in drinking water and its ill affect on human health: a review. J. Tissue Res. 4, 263–273.

Ioannidou, O., Zabaniotou, A., 2007. Agricultural residues as precursors for activated carbon production – a review. Renew. Sustain. Energy Rev. 11, 1966–2005.

Kabay, N., Arar, O., Samatya, S., Yüksel, U., Yüksel, M., 2008. Separation of fluoride from aqueous solution by electrodialysis: effect of process parameters and other ionic species. J. Hazard. Mater. 153, 107–113.

Killedar, D.J., Bhargava, D.S., 1993. Effect of stirring rate and temperature on fluoride removal by fishbone charcoal. Indian J. Environ. Health 35, 81–87.

Kolodynska, D., Wnetrzak, R., Leahy, J.J., Hayes, M.H.B., Kwapinski, W., Hubicki, Z., 2012. Kinetic and adsorptive characterization of biochar in metal ions removal. Chem. Eng. J. 197, 295–305.

Lagergren, S., 1898. Zur theorie der sogenannten adsorption geloster stoffe Kungliga Svenska Vetenskapsakademiens. Handligar 24, 1–39.

Langmuir, I., 1916. The constitution and fundamental properties of solids and liquids. J. Am. Chem. Soc. 38, 2221–2295.

Lesmana, S.O., Febriana, N., Soetaredjo, F.E., Sunarso, J., Ismadji, S., 2009. Studies on potential applications of biomass for the separation of heavy metals from water and wastewater. Biochem. Eng. J. 44, 19–41.

Lu, H., Zhang, W., Yang, Y., Huang, X., Wang, S., Qiu, R., 2012. Relative distribution of Pb2+ sorption mechanisms by sludge – derived biochar. Water Res. 46, 854–862.

Mattson, J.S., Mark, H.B., 1971. Activated Carbon: Surface Chemistry and Adsorption from Aqueous Solution. Marcel Dekker, New York.

Meenakshi, S., Maheswari, R.C., 2006. Fluoride in drinking water and its removal. J. Hazard. Mater. B137, 456–463.

Mohan, D., Sharma, R., Singh, V.K., Steele, P., Pittman Jr., C.U., 2012. Fluoride removal from water using bio-char, a green waste, low-cost adsorbent: equilibrium uptake and sorption dynamics modeling. Ind. Eng. Chem. Res. 51, 900–914.

Msagati, T.A.M., Mamba, B.B., Sivasankar, V., Omine, K., 2014. Surface restructuring of lignite by bio-char of cuminum cyminum – exploring the prospects in defluoridation followed by fuel applications. Appl. Surface Sci. 301, 235–243.

Murray, J.W., Stumm, W. (Eds.), 1988. Aquatic Surface Chemistry: Chemical Processes at the Particle-Water Interface. John Wiley & Sons, New York, 52, 1742.

Newcombe, G., Hayes, R., Drikas, M., 1993. Granular activated carbon: importance of surface properties in the adsorption of naturally occurring organics. Colloids Surf. A: Physicochem. Eng. Aspects 78, 65–71.

Oh, T.-K., Choi, B., Shinogi, Y., Chikushi, Y., 2012. Effect of pH conditions on actual and apparent fluoride adsorption by biochar in aqueous media. Water Air Soil Pollut. 223, 3729–3738.

Pakula, M., Walczyk, M., Biniak, S., Swiatkowski, A., 2007. Electrochemical and FTIR studies of the mutual influence of lead (II) and iron (II) and phenol on their adsorption from aqueous acid solution by modified activated carbons. Chemosphere 69, 209–219.

Patnukao, P., Pavasant, P., 2008. Activated carbons from Eucalyptus camaldulensis Dehn bark using phosphoric acid activation. Bioresource Technol. 99, 8540–8543.

Paudyal, H., Pangeni, B., Inoue, K., Kawakita, H., Ohto, K., Ghimire, K.N., Alam, S., 2013. Preparation of novel alginate based anion exchanger from Ulva japonica and its application for the removal of trace concentrations of fluoride from water. Bioresource Technol. 148, 221–227.

Prasad, R., 1993. Fuel Efficient Cook Stores Using Cow Dung Cakes, Boiling Point, Issue 30 Soles and Subsides. Centre for Rural Development and Appropriate Technology, IIT, New Delhi.

Sasaki, K., Yoshida, M., Ahmmad, B., Fukumoto, N., Hirajima, T., 2013. Sorption of fluoride on partially calcined dolomite. Colloid Surf A: Physicochem. Eng. Aspects 435, 56–62.

Sepehr, M.N., Sivasankar, V., Zarrabi, M., Senthil Kumar, M., 2013. Surface modification of pumice enhancing its fluoride adsorption capacity: an insight into kinetic and thermodynamic studies. Chem. Eng. J. 228, 192–204.

Shen, D., Xiao, R., Gu, S., Luo, K., 2011. The pyrolytic behavior of cellulose in lignocellulosic biomass: a review. RSC Adv. 1, 1641–1660.

Sivabalan, R., Rengaraj, S., Banumathi, A., Murugesan, V., 2002. Fluoride uptake characteristics of activated carbon from agricultural-waste. J. Sci. Ind. Res. 61, 1039–1045.

Sivasankar, V., Ramachandramoorthy, T., Darchen, A., 2011. Manganese-oxide improves the efficiency of earthenware in fluoride removal from drinking water. Desalination 272, 179–186.

Sivasankar, V., Rajkumar, S., Murugesh, S., Darchen, 2012a. A influence of shaking or stirring dynamic methods in the defluoridation behavior of activated tamarind fruit shell carbon. Chem. Eng. J. 197, 162–172.

Sivasankar, V., Rajkumar, S., Murugesh, S., Darchen, A., 2012b. Tamarind (Tamarindus indica) fruit shell carbon: a calcium-rich promising adsorbent for fluoride removal from ground water. J. Hazard. Mater. 225–226, 164–172.

Sivasankar, V., Murugesh, S., Rajkumar, S., Darchen, 2013. A Cerium Dispersed in Carbon (CeDC) and its adsorption behavior: a first example of tailored adsorbent for fluoride removal from drinking water. Chem. Eng. J. 214, 45–54.

Swain, S.K., Padhi, T., Patnaik, T., Patel, R.K., Jha, U., Dey, R.K., 2010. Kinetics and thermodynamics of fluoride removal using cerium-impregnated chitosan. Desalination Water Treat. 13, 369–381.

Tahaikt, M., El Habbani, R., Ait Haddou, A., Achary, I., Amor, Z., Taky, M., Alami, A., Boughriba, A., Hafsi, M., Elmidaoui, A., 2007. Fluoride removal from groundwater by nanofiltration. Desalination 212, 46–53.

Tang, Q.Q., Du, J., Ma, H.H., Jiang, S.J., Zhou, X.J., 2008. Fluoride and children's intelligence: a meta-analysis. Biol. Trace Elem. Res. 126, 115–120.

Tchomgui-Kamga, E., Alonzo, V., Nanseu-Njiki, C.-P., Audebrand, N., Ngameni, E., Darchen, A., 2010a. Preparation and characterization of charcoals that contain dispersed aluminum oxide as adsorbents for removal of fluoride from drinking water. Carbon 48, 333–343.

Tchomgui-Kamga, E., Ngameni, E., Darchen, A., 2010b. Evaluation of removal efficiency of fluoride from aqueous solution using new charcoals that contain calcium compounds. J. Colloid. Interface Sci. 346, 494–499.

Tripathy, S.S., Bersillon, J.L., Gopal, K., 2006. Removal of fluoride from drinking water by adsorption onto alum-impregnated activated alumina. Sep. Purif. Technol. 50, 310–317.

Vinod, V.P., Anirudhan, T.S., 2001. Sorption of tannic acid on zirconium pillared clay. J. Chem. Technol. Biotechnol. 77, 92–101.

Weber, W.J., Morris, J.C., 1964. Equilibria and capacities for adsorption on carbon. J. Sanitary Eng. Div. 90, 79–107.

World Health Organisation, 2004. Guidelines for Drinking Water Quality (vol. 2) Health Criteria and other Supporting Information, second ed., Genova, pp. 231–233.

Winterhalder, B., Larsen, R., Thomas, R.B., 1974. Dung as an essential resource in a highland Peruvian community. Human Ecol. 2, 89–104.

Yadhav, A.K., Abbassi, R., Gupta, A., Dadashzadeh, M., 2013. Removal of fluoride from aqueous solution and groundwater by wheat straw, saw dust and activated baggasse carbon of sugar cane. Ecol. Eng. 52, 211–218.

Yu, X., Tong, S., Ge, M., Zuo, J., 2013. Removal of fluoride from drinking water by cellulose@hydroxyapatite nanocomposites. Carbohydrate Polym. 92, 269–275.